Polymer-Plastics Technology and Engineering

Morphology and Mechanical Properties of iPP/Silica Composites Modified with (Styrene-b-ethylene-co-butylene-b-styrene) Grafted with Maleic Anhydride

Anđela Pustak[a], Matjaž Denac[b], Mirela Leskovac[c], Iztok Švab[d], Vojko Musil[b] & Ivan Šmit[a]

[a] Division of Materials Chemistry, Rudjer Bošković Institute, Zagreb, Croatia

[b] FEB Maribor, Institute of Technology, University of Maribor, Maribor, Slovenia

[c] Faculty of Chemical Engineering and Technology, University of Zagreb, Zagreb, Croatia

[d] ISOKON, Production and Processing of Thermoplastics, Ltd., Slovenske Konjice, Slovenia
Accepted author version posted online: 06 Jan 2015.

PLEASE SCROLL DOWN FOR ARTICLE

Taylor & Francis
Taylor & Francis Group

Morphology and Mechanical Properties of iPP/Silica Composites Modified with (Styrene-*b*-ethylene-*co*-butylene-*b*-styrene) Grafted with Maleic Anhydride

Anđela Pustak[1], Matjaž Denac[2], Mirela Leskovac[3], Iztok Švab[4], Vojko Musil[2], and Ivan Šmit[1]

[1]*Division of Materials Chemistry, Rudjer Bošković Institute, Zagreb, Croatia*
[2]*FEB Maribor, Institute of Technology, University of Maribor, Maribor, Slovenia*
[3]*Faculty of Chemical Engineering and Technology, University of Zagreb, Zagreb, Croatia*
[4]*ISOKON, Production and Processing of Thermoplastics, Ltd., Slovenske Konjice, Slovenia*

GRAPHICAL ABSTRACT
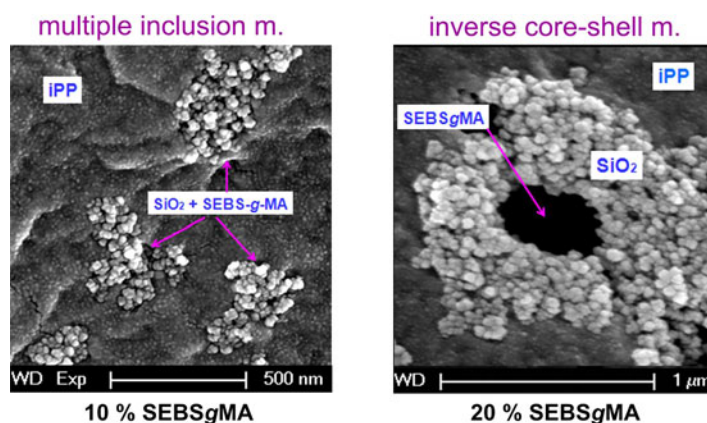
The effects of different silica grades and elastomer content on interfacial properties, morphology and mechanical properties of polypropylene/silica 96/4 composites modified with added 5, 10, 15, and 20% of poly(styrene-*b*-ethylene-*co*-butylene-*b*-styrene) grafted with maleic anhydride (SEBS-*g*-MA) were investigated. The iPP/silica/SEBS-*g*-MA composites were designed by adding four silica fillers differing in size (nano- *vs*. micro-) and in surface properties (hydrophilic *vs*. hydrophobic) and SEBS-*g*-MA that was used as a proven effective impact modifier and compatibilizer simultaneously. The morphology of every composite was a spectrum of several morphologies rather than one exclusive morphology. Good concordance between observed and predicted morphology indicated that the morphology of a particular composite was controlled primarily by interfacial properties. Tensile and impact properties were influenced primarily by competitive effects of a stiff filler and tough SEBS-*g*-MA elastomer. Increased impact strength and strain at break caused by adding SEBS-*g*-MA indicated a significant overcoming of the elastomeric toughening effect in relation to the filler's stiffening effect.

Keywords Interfacial properties; Mechanical properties; Morphology; Polypropylene Composites

INTRODUCTION

The production of polymer-matrix composites has grown intensely owing to a favourable cost/performance ratio and simple fabrication methods.[1,2] A remarkable progress in polymer composites as advanced materials has been achieved through functionalization of filler surfaces and introduction of

nanofillers. Among polyolefins, isotactic polypropylene (iPP) is one of the most widely used commodity plastomers due to its outstanding properties and versatile applications of its composites. On the other hand, among synthetic fillers, silica (SiO_2) offers some improvements in terms of the processability and mechanical properties of polymer composites.[1–3]

Most published studies of the iPP/SiO_2 systems are related to the binary iPP/silica nanocomposites with two aims in mind: the crystallization study of these composites and the improvement of their mechanical properties mainly by silica surface modification. As the incorporation of a filler into the polymer matrix usually enhances the stiffness and deteriorates the impact strength, a rubber toughening agent and an appropriate compatibilizer should be added in order to improve the interface stress transfer and to balance toughness and stiffness to get a satisfying cost-property performance ratio of material.[1,2] However, the efficiency of rubber impact modifiers and compatibilizing agents between the filler and the matrix for the iPP/silica composites has been rarely investigated.[4–8]

Bikiaris et al. have accomplished a very efficient compatibilization of the iPP/nanosilica composites by polypropylene functionalized with maleic anhydride (PP-g-MA) manifested in enhanced mechanical properties with the silica agglomerate reduction.[4] Chen et al.[5] have combined compatibilization with toughening in a proposed hybrid composite system of polypropylene with silica and polyurethane (PU) (PP/PP-g-NH_2/SiO_2-g-PU/PU). The impact strength and ductility of these hybrid composites have been improved[5]. Uotila et al. [6] have established a uniform dispersion of microsilica particles and aggregates throughout the iPP/EPR blend, e.g., their selectivity for both phases. Although ethylene/butyl acrylate (E/BA) and ethylene/butyl acrylate/maleic anhydride (E/BA/MAH) compatibilizer encapsulated EPR and dragged the filler particle towards the EPR phase, in composites with PP-g-MAH compatibilizer the microsilica particles were dominantly dispersed throughout the iPP matrix forming a phase-separated morphology.

In the iPP/EPDM/nanosilica composites Martin et al.[7] observed that hydrophilic silica aggregates tend to migrate within the elastomeric EPDM phase, whereas hydrophobic particles are homogeneously dispersed within the EPDM phase and at the PP-silica interface. The investigation of Bazgir et al.[8] on dynamically cross-linked EPDM/iPP 60/40 blends filled with silica has shown that silica tends to remain encapsulated by the EPDM rubber when mixed with EPDM before the addition of iPP. Encapsulated silica particles changed the EPDM/iPP viscosity ratio, and thereby the size of EPDM droplets and mechanical properties of composites.

Liu and Kontopoulou[9] observed better filler dispersion by addition of PP-g-MA and reduction of large silica aggregates. Silica was located preferentially in PP/PP-g-MA phase and this separated morphology as well as elastomeric ethylene-octene copolymer (POE) lead to impact properties improvement and stiffness-toughness balance. Wang and Liu[10] concluded that

the stiffness-toughness balance of the iPP/silica/SBR composites has been established due to a strong synergistic factor between the filler and the elastomer.

Mae et al.[11] observed that the elastic modulus and the strain values of iPP/SiO_2 composites modified with poly (styrene-b-ethylene-co-butylene-b-styrene) (SEBS) depended on the selectivity of SiO_2 nanoparticles, i.e., are they inside or outside of dispersed elastomeric SEBS particles.

The most recent investigations of the iPP/SiO_2/SEBS composites with PP-g-MA added as compatibilizer by Panaitescu et al.[12,13] confirmed relatively good compatibility of the iPP/SEBS interface resulting in improvement of mechanical and dielectrical properties. The location of filler and interactions played again a crucial role in determing the properties of such composite systems.

On the other side, Midany and Ibrahim[14] used poly(styrene-b-ethylene-co-butylene-b-styrene) (SEBS) and maleated SEBS (SEBS-g-MA) as compatibilizers. Remarkable improvement in impact strength and strain was attributed to the interaction between silica particles and compatibilizer, due to good compatibilization of the iPP/SiO_2 interface by added elastomer.[14]

Although a lot of studies have already been published on morphology and mechanical properties of iPP/silica composites,[4–8] no thorough study on their adhesion properties and relation to the composite morphology has been conducted. Although the filler selectivity has been investigated in the ternary polymer composites[6–14], no inverse core-shell morphology with full-scale filler interphase/interlayer between the two polymers has been observed. Therefore, the relation between the adhesion properties and the ultimate morphology of compression molded iPP/silica composites modified with styrenic block copolymer poly(styrene-b-ethylene-co-butylene-b-styrene) grafted with maleic anhydride (SEBS-g-MA) has been studied. Research was carried out with silica fillers differing in size (nano- vs. micro-) and surface properties (hydrophilic vs. hydrophobic, e.g., polar vs. nonpolar). SEBS-g-MA was used as a proven effective impact modifier and compatibilizer simultaneously. The effects of different silica fillers on the morphology and mechanical properties of composites were discussed in the context of adhesion-morphology-mechanical property relationships.

EXPERIMENTAL

Materials

The materials used in this investigation were isotactic polypropylene (iPP) as a matrix, poly(styrene-b-ethylene-co-butylene-b-styrene) block copolymer grafted with maleic anhydride (SEBS-g-MA with 2% of MA) as a compatibilizer and elastomeric impact modifier, and four types of silica fillers. Two proprietary microsilicas (unmodified Sipernat 120 and surface-modified Sipernat D17) and two proprietary nanosilicas (unmodified Aerosil 200 and surface-modified silica Aerosil R7200) were used. The properties of used polymers and fillers are listed in Table 1.

TABLE 1
The properties of used materials

Polymer	Trade name	Density[a] (g cm⁻³)	MFI (g10⁻¹ min⁻¹)	M_n^d (gmol⁻¹)	$M_w/M_n{}^d$
iPP	Moplen HP501 L	0.90	6.0[b]	120,000	5.4
SEBS-g-MA (2% of MA)	Kraton KG-1901	0.91	3.1[c]	47,300	1.55

Filler	Trade name	Tapped density[a] (g L⁻¹)	Surface modification[a]	Specific surface area[a] (m²g⁻¹)	Particle size[a], d_{50}
S-120 microsilica	Sipernat 120	185	none	125	14.5 µm
S-D17 microsilica	Sipernat D17	150	2% of chem. bonded carbon	100	10 µm
A-200 nanosilica	Aerosil 200	∼50	none	200	12 nm
A-R7200 nanosilica	Aerosil R7200	∼230	methacryl-silane	150	12 nm

[a]According to producer declaration.
[b]According to ISO 1133 (230°C/2.16 kg).
[c]According to ISO 1133 (200°C/5 kg).
[d]Measured by exclusion chromatography against the PS standard.

Sample Preparation

Ternary iPP/SiO₂/SEBS-g-MA composites were prepared in a Brabender kneading chamber. The elastomer concentration was varied to 5, 10, 15 and 20% of SEBS-g-MA elastomer per hundred composite parts of iPP/SiO₂ with a constant ratio 96/4. The volume content ratio iPP/SiO₂ 96/4 was chosen because all binary iPP/SiO₂ composites exhibit the best spherulitic morphology and tensile strength values in the silica content range $2 - 6\%$.[15,16] A relatively wide (0–20%) SEBS-g-MA elastomer content range was used in order to explore its efficiency as impact modifier (not only as compatibilizer). The components were put into the kneading chamber preheated up to 200°C with the rotor speed of 50 min⁻¹, then kneaded for 7 min. After homogenization, the melt was rapidly transferred to a preheated laboratory press and compression molded into 1- and 4-mm-thick plates. The pressing temperature was 220°C, and the pressing time 14 min for 1-mm and 11.5 min for 4-mm-thick plates under a pressure progressively increased up to 100 bar.

Testing Methods

Contact Angle Measurement

Surface free energies, as well as the corresponding dispersive and polar component of materials, were determined by measuring the contact angles. The contact angles of the iPP polymer, the SEBS-g-MA elastomer and silica fillers were measured on a contact angle goniometer, DataPhysics OCA 20 Instrument, at a temperature of 23°C. Contact angle measurements were done on 1-mm thick plates of neat iPP and SEBS-g-MA polymers and on the pellets of the silica fillers. Sessile drops (2 µL) of test liquids: water (twice distilled $\lambda = 1.33\,\mu\text{Lcm}^{-1}$), formamide (p.a. 99.5%, Fluka) and diiodomethane (p.a. 99%, Aldrich) were used for the advancing contact angle measurements. The average values of at least five drops at different places of the same sample were taken and the standard deviation was always less than 2%. The surface tensions of the test liquids used for the contact angle measurements are shown in Table 2.

Surface free energies of the iPP and silica fillers (γ_s) were calculated using the harmonic mean equation[19] according to Wu's model (1):

$$\gamma_l(1 + \cos\theta) = \frac{4\gamma_s^d\gamma_l^d}{\gamma_s^d + \gamma_l^d} + \frac{4\gamma_s^p\gamma_l^p}{\gamma_s^p + \gamma_l^p} \tag{1}$$

where γ_l and γ_s are the surface energies of liquid and solid, respectively, the superscript d refers to the dispersive and p to the polar component, and θ is the measured contact angle.

Steady-State Torque Moment

The torque value (T_M) was determined from the diagram of kneading in the Brabender kneading chamber. The average T_M value was calculated on the basis of 5 measurements carried out for each sample.

TABLE 2
Surface free energy (γ_l), dispersion (γ_l^d), and polar component (γ_l^p) of test liquids for contact angle measurements[17,18]

Test liquids	γ_l (mJ m⁻²)	γ_l^d (mJ m⁻²)	γ_l^p (mJ m⁻²)
Water	72.8	21.8	51.0
Formamide	58.0	39.0	19.0
Di-iodomethane	50.8	50.8	0.0

Scanning Electron Microscopy (SEM)

A SIRION 400 NC scanning electron microscope (SEM) was used to study the morphology of ternary composites. Samples were cryofractured and gold-plated before being examined with a microscope at an acceleration voltage up to 10 kV at various magnifications. All SEM micrographs are secondary electron images.

Tensile Tests

Tensile properties were measured according to ISO 527 using Zwick 147670 Z100/SN5A apparatus at 23°C and a constant strain rate of 2 mm min^{-1}. For each sample, five measurements were taken and average values calculated.

Notched Impact Strength

The notched impact strength was measured by Zwick apparatus at 25°C according to the Charpy test (DIN 53453). For each sample 12 measurements were taken and average values calculated within the standard deviation of 5%.

Optical Microscopy (OM)

A Leica light microscope (Model DMLS) connected to a digital camera was used for observation of thin crossed microtomed sections (taken from 1-mm-thick plates) under crossed polarizers (POM) or phase contrast (PC). The maximum anisotropic diameter of spherulites ($d_{i,\max}$) was measured on several polarization micrographs of each sample and the average spherulite diameter (d_{sph}) calculated according to Eq. (2):

$$d_{sph} = \frac{\sum N_i d_{imax}}{\sum N_i} \quad (2)$$

where N_i is the number of measured spherulites with the average diameter d_i.

RESULTS AND DISCUSSION
Interfacial Properties of the iPP/SiO$_2$/SEBS-g-MA Composites

The properties of multiphase systems such as polymer composites and blends are determined by the characteristics of their constituents, composition, structure and interfacial interaction. Key factors determining the preferential localization of fillers and elastomeric modifiers, and the particular morphology of multiphase polymer composites, are thermodynamic, kinetic, and polymer melt viscosity.[20] Different approaches based on thermodynamic considerations allow prediction of interfacial interactions and the resulting morphology of multiphase systems. These approaches mainly include the interactivity values between phases in binary and ternary composites[19,20].

The domain morphology of ternary polymer blends and composites could be classified as separated, core-shell and stacked[21,22]. The appearance of the inverse core-shell (iCS) and compartmentalized core-shell morphology could also be assumed; the latter is known under different names: morel structure, honeycomb-like morphology, and multiple inclusion or salami-like morphology[23]. The inverse core-shell morphology fully contains an interlayer of agglomerated particles that encapsulates dispersed elastomer particles in the polymer matrix in distinct to sporadic nanoparticles or agglomerates at the interface[7]. The ultimate ideal morphologies of the iPP/SiO$_2$/SEBS-g-MA composites may be predicted by analyzing the adhesion parameters (interfacial free energy, adhesion work, spreading coefficient).

Adhesion Parameters of the iPP/Silica/SEBS-g-MA Composites

The contact angle measurement is a standard method for evaluating the surface free energies (γ) and their dispersive (γ^d) and the polar component (γ^p) of solids[19]. Surface free energies as well as their dispersive and polar component of the iPP, SEBS-g-MA and different silica fillers were calculated using the harmonic mean equation (1) (Wu's model) are given in Table 3.

The calculation of adhesion parameters such as interfacial free energy, γ_{AB}, the thermodynamic work of adhesion, W_{AB}, and the spreading coefficient, S_{AB}, represented in Eqs. (3–6) can be used to predict possible component interactions at the polymer/elastomer, polymer/filler and elastomer/filler interface of binary systems[19]. The adhesion parameters between different components of iPP/silica/SEBS-g-MA composites for possible polymer/elastomer, polymer/filler and elastomer/filler pairs have been calculated from the obtained γ values and presented in Table 4:

$$\gamma_{AB} = \gamma_A + \gamma_B - 2\sqrt{\gamma_A^d \gamma_B^d} - 2\sqrt{\gamma_A^p \gamma_B^p} \quad (3)$$

$$\gamma_{AB} = \gamma_A + \gamma_B - \frac{4\gamma_A^d \gamma_B^d}{\gamma_A^d + \gamma_B^d} + \frac{4\gamma_A^p \gamma_B^p}{\gamma_A^p + \gamma_B^p} \quad (4)$$

TABLE 3

Surface free energies and their dispersive and polar components of iPP, SEBS-g-MA and different silica filler evaluated by using the harmonic mean equation

Component	Surface free energy (mJ m^{-2})			Polarity (%)
	γ	γ^d	γ^p	
iPP	32.8	31.5	1.3	3.9
SEBS-g-MA	36.3	26.2	10.1	27.8
S-120	74.6	37.6	37.0	49.6
S-D17	7.3	7.3	0.0	0.0
A-200	76.7	39.6	37.1	48.4
A-R7200	61.2	43.4	17.8	29.1

Polarity - $\gamma^p/\gamma \cdot 100$ (percentage of polar component in overall surface free energy).

$$W_{AB} = \gamma_A + \gamma_B - \gamma_{AB} \qquad (5)$$

$$S_{AB} = \gamma_B - \gamma_A - \gamma_{AB} \qquad (6)$$

where subscripts A refer to the matrix (major phase) and B to the dispersed (minor phase) such as filler or elastomer phases.

The results of the studies on the effective adhesion between component pairs indicate some conditions as optimal: the thermodynamic work of adhesion as maximal, the spreading coefficient as a positive value and interfacial free energy or interfacial tension as a minimal one[19,20,24]. If these conditions are met, the established interactions between component pairs point to the strength of adhesion in binary systems. They may also indicate which interface in a ternary system could exhibit the most effective adhesion.

As the adhesion work values and the spreading coefficient sometimes lead to incoherent conclusions[25,26], the interfacial free energy values seemed to be more relevant for ambiguous systems. The interfacial free energy between the iPP polymer and the untreated microfiller S-120 and untreated nanosilica filler A-200 is very high (Table 4), which indicates the preferable filler dispersion in the iPP matrix and the probability of preferential separated morphology (SM). Otherwise, the lower interfacial energy between the S-120 and A-200 filler and SEBS-g-MA indicate the filler distribution in the elastomer

TABLE 4
The adhesion parameters between different components of iPP/SiO$_2$/SEBS-g-MA composite for possible adhesion pairs: polymer/elastomer, polymer/filler or elastomer/filler

Possible adhesion pairs	Adhesion parameters (mJ m^{-2})			
	Interfacial free energy $\gamma_{\mathbf{AB}}$		Work of adhesion $W_{\mathbf{AB}}$*	Spreading coefficient $S_{\mathbf{AB}}$*
	Eq. (3)	Eq. (4)		
iPP/SEBS-g-MA	4.44	7.28	64.60	−1.00
iPP/S-120	24.69	33.82	82.69	17.09
SEBS-g-MA/ S-120	9.46	17.40	101.43	28.83
iPP/S-D17	9.77	16.39	30.33	−35.27
SEBS-g-MA/ S-D17	15.90	20.76	27.66	−44.94
iPP/A-200	24.97	34.31	84.51	18.91
SEBS-g-MA/ A-200	9.86	18.19	103.13	30.53
iPP/A-R7200	10.43	16.15	83.57	17.97
SEBS-g-MA/ A-R7200	3.24	6.37	94.26	21.66

A-matrix, B-elastomer or filler (3) geometric mean equation; (4) harmonic mean equation; *γ_{AB} calculated from geometric mean Eq. (3).

phase and the probability of preferential core-shell morphologies (CS and cCS).

The spreading coefficient is a quantitative measure of wetting which allows us to predict whether one phase spontaneously spreads on the surface of another. The positive values of the spreading coefficient indicate wetting as well as good adhesion at the interface between two phases, whereas negative values indicate dewetting and low adhesion between phases. The positive values of the spreading coefficient S_{AB} (Table 4) of components pairs SEBS-g-MA/S-120 and SEBS-g-MA/A-200 indicate preferential core-shell morphologies (CS and cCS) in both the iPP/S-120/SEBS-g-MA and the iPP/A-200/SEBS-g-MA ternary composites.

Interfacial Free Energy of iPP/Silica/SEBS-g-MA Composites

Prediction of filler particles location: according to thermodynamic approach, the filler (F) will be located at the interface of two polymers (A and B) if two conditions are met:[27]

1. migration of fillers from phase A to the interface:

$$\gamma_{AF} > \gamma_{BF} - \gamma_{AB}/2 \qquad (7)$$

2. migration of fillers from phase B to the interface:

$$\gamma_{BF} > \gamma_{AF} - \gamma_{AB}/2 \qquad (8)$$

where γ_{AF} and γ_{BF} are the filler's specific excess interfacial free energies in components A and B, respectively, whereas γ_{AB} is the polymers specific excess interfacial free energy. γ_{AF} and γ_{BF} values, obtained by calculating with Eqs. (7) and (8), are presented in Table 5.

According to the results shown in Table 5, unmodified S-120, A-200 silica fillers and modified A-R7200 nanosilica with polar surfaces distribute selectively in the polar SEBS-g-MA elastomer phase, thus allowing the formation of the encapsulated core-shell morphologies (CS, cCS). Moreover, the modified non-polar silica S-D17 tends to migrate from SEBS-g-MA elastomer in the matrix iPP phase, thus forming a separated morphology (SM). However, the composites with treated surface silica fillers S-D17 and A-R7200 exhibit smaller differences between γ_{AF} and $\gamma_{BF} - \gamma_{AB}/2$ values (Table 5) (S-D17: $\gamma_{AF} = 9.77$, $\gamma_{BF} - \gamma_{AB}/2 = 12.26$; A-R7200: $\gamma_{AF} = 3.24$, $\gamma_{BF} - \gamma_{AB}/2 = 6.76$) than the composites with other two silica fillers (S-120: $\gamma_{AF} = 24.69$, $\gamma_{BF} - \gamma_{AB}/2 = 5.82$; A-200: $\gamma_{AF} = 24.97$, $\gamma_{BF} - \gamma_{AB}/2 = 6.22$). This fact might indicate a higher migration tendency of the S-D17 and A-R7200 fillers to the interface with the formation of the inverse core-shell morphology (iCS).

The Wetting Coefficient of iPP/Silica/SEBS-g-MA Composites

According to the qualitative approach proposed by Sumita et al.[28] the wetting coefficient (ω_a) that allows predicting

TABLE 5
According to the thermodynamic approach, the filler migrates to the A-B interface when conditions are met (Yes)

Ternary polymer composites	$\gamma_{AB}/2$	γ_{AF}	γ_{BF}	$\gamma_{BF} - \gamma_{AB}/2$	$\gamma_{AF} - \gamma_{AB}/2$	$\gamma_{AF} \geq \gamma_{BF} - \gamma_{AB}/2$	$\gamma_{BF} \geq \gamma_{AF} - \gamma_{AB}/2$
iPP/S-120/SEBS-*g*-MA	3.64	24.69	9.46	5.82	21.05	Yes	No
iPP/S-D17/SEBS-*g*-MA	3.64	9.77	15.9	12.26	6.13	No	Yes
iPP/A-200/SEBS-*g*-MA	3.64	24.97	9.86	6.22	21.33	Yes	No
iPP/A-R7200/SEBS-*g*-MA	3.64	10.43	3.24	−0.43	6.79	Yes	No

A-matrix, B-elastomer, F-filler, γ_{AB} according to Wu's Eq. (4), γ_{AF}, γ_{BF} according to geometric mean Eq. (3).

the filler selectivity in a ternary system is calculated by Eq. (9):

$$\omega_a = \frac{\gamma_{BF} - \gamma_{AF}}{\gamma_{AB}} \qquad (9)$$

where γ_{AF} and γ_{BF} are the interfacial tensions between the filler and the polymer A or B, and γ_{AB} is the interfacial tension between polymers A and B.

According to this approach:

$\omega_a > 1 \rightarrow$ filler particles located within phase A
$\omega_a < -1 \rightarrow$ filler particles located within phase B
$-1 < \omega_a < 1 \rightarrow$ filler particles distributed at the interface

The interfacial free energy, wetting coefficient and location of the filler for the ternary polymer composite components are presented in Table 6.

According to the results shown in Table 6, unmodified silica fillers S-120 and A-200 remain in the elastomeric SEBS-*g*-MA phase allowing preferential formation of the core-shell morphology varieties (CS, cCS). Conversely, modified microsilica S-D17 and nanosilica AR7200 are located preferentially in the interphase forming the inverse core-shell morphology (iCS).

The Spreading Coefficient of iPP/Silica/SEBS-g-MA Composites

Hobbs et al.[29] used the Harkins spreading coefficient concept for interpreting or predicting the morphology of different ternary blends. For a ternary system with A as the matrix phase and B and F as the dispersed elastomer and filler phases, the spreading coefficient λ_{AF} of the A-phase on the F-phase is

simply derived by Eq. (10):

$$\lambda_{AF} = \gamma_{BF} - \gamma_{AB} - \gamma_{AF} \qquad (10)$$

where γ_{BF} is the interfacial tension between B and F phases, γ_{AB} is the interfacial tension between A and B phases, γ_{AF} is the interfacial tension between B and F phases.

If $\lambda_{AF} > 0$, the A-phase will encapsulate the F-phase while $\lambda_{AF} < 0$ indicates separated phases A and F. The λ_{AF} tends to null if the F (filler) migrates to interphase between the A and B phases. The results are presented in Table 7.

The highest positive Harkins spreading coefficient values, λ_{AF}^*, for composites with untreated polar fillers S-120 (micro) and A-200 (nano) (Table 7) indicate good interactions between dispersed filler and SEBS-*g*-MA elastomer particles. Accordingly, core-shell morphologies (CS and cCS) seem to be more probable than iCS and SM morphologies in these systems. Since the negative λ_{AF} values of the iPP/S-D17/SEBS-*g*-MA and iPP/A-R7200/SEBS-*g*-MA composites tend to zero, a tendency of interphase location of the S-D17 and A-R7200 fillers could be assumed, i.e., the inverse core-shell morphology (iCS). A somewhat lower negative λ_{AF} value for a composite with SD17 ($\lambda_{AF} = -1.15$) compared with those with A-R7200 filler ($\lambda_{AF}^* = -0.09$) (Table 7) may indicate a slightly stronger tendency of the S-D17 than the A-R7200 filler toward the formation of phase-separated morphology (SM).

Predicted Morphologies of iPP/SiO₂/SEBS-g-MA Composites

Based on the analysis of the results in Tables 4–7, the most likely morphologies in these composites could be assumed. Predicted morphologies in the presented iPP/SiO₂/SEBS-*g*-MA composites are rather a spectrum of all possible

TABLE 6
Filler location calculated according to the wetting coefficient approach [Eq. (9)]

Ternary polymer composites	γ_{AB}	γ_{AF}	γ_{BF}	ω_A	Filler location
iPP/S-120/SEBS-*g*-MA	7.28	24.69	9.46	−2.09	Phase B (SEBS-*g*-MA)
iPP/S-D17/SEBS-*g*-MA	7.28	9.77	15.90	0.84	Interphase
iPP/A-200/SEBS-*g*-MA	7.28	24.97	9.86	−2.08	Phase B (SEBS-*g*-MA)
iPP/A-R7200/SEBS-*g*-MA	7.28	10.43	3.24	−0.99	Interphase

A-matrix, B-elastomer, F-filler, γ_{AB} according to the harmonic mean Eq. (4), γ_{AF}, γ_{BF} according to the geometric mean Eq. (3).

TABLE 7

Harkins spreading coefficients of ternary hybrid polymer composites calculated by Eq. (10). The filler migrates to the interface when the spreading coefficient (λ_{AF} or λ_{AF}^*) is close to zero

Ternary polymer composites	γ_{AB}	γ_{AF}	γ_{BF}	λ_{AF}	λ_{AF*}
iPP/S-120/SEBS-g-MA	7.28	24.69	9.46	−22.51	7.95
iPP/S-D17/SEBS-g-MA	7.28	9.77	15.90	−1.15	−13.41
iPP/A-200/SEBS-g-MA	7.28	24.97	9.86	−22.39	7.83
iPP/A-R7200/SEBS-g-MA	7.28	10.43	3.24	−14.47	−0.09

γ_{AB} according to the harmonic mean Eq. (4), γ_{AF}, γ_{BF} according to the geometric mean Eq. (3); A - iPP matrix, B - elastomer, F – filler; *A-elastomer, B-iPP matrix, F-filler.

morphologies: CS, cCS, iCS, and SM (Table 8). These results are in line with literature findings that the filler is not fully located in one phase but migrates to a certain extent into the second polymer and/or at the iPP—SEBS-g-MA interface[24].

However, the results in Table 8 indicate one or possibly two dominant morphology types in every composite. Accordingly, compartmentalized core-shell or multiple inclusion morphology (cCS) predominate in the composites with polar S-120 microsilica and A-200 nanosilica containing -OH groups at the surface of silica particles. On the other hand, the inverse core-shell morphology (iCS) prevails in the composites containing S-D17 microsilica and A-R7200 nanosilica fillers with modified surfaces (Table 8). Moreover, iPP composites with a nanosilica A-R7200 filler seem to exhibit a full spectrum of possible morphologies: CS, cCS, iCS, and SM.

Steady-State Torque Moment of iPP Composites

The torque value provides information on how the SEBS-g-MA modifier influences the processabillity of iPP/silica composites. The torque moment increases by adding components in batch mixer and decreases after the polypropylene melting and reaches constant value around sixth minute of mixing (T_M values in Fig. 1 are measured at 7 min) due to homogenization and equalized viscosity of composites. The torque moment value (T_M) can be considered a measure of the viscosity under the same mixing conditions. The T_M values of iPP composites change slightly (in the case of untreated

S-120 and A-200 fillers) or even negligibly (in the case of modified S-D17 and A-R7200 fillers).

That is to say, uncoated/untreated fillers in binary iPP/silica composites contribute to higher melt viscosity than coated/treated fillers do (at $\varphi_{SEBS-g-MA} = 0\%$ in Fig. 1). However, T_M values of the composites with microsilicas as well as those with nanosilicas approach each other with an increase in the SEBS-g-MA content. Such convergence indicates the intensifying factor of the particle size in relation to the filler surface properties on melt viscosity with an increase in the elastomer content. As a result, molten composites with microsized filler particles exhibit somewhat higher viscosity than those with nanosized filler particles, which corresponds to the findings of Das et al.[30]

Morphology of iPP/SiO$_2$/SEBS-g-MA Composites

Scanning Electron Microscopy (SEM)

SEM and TEM micrographs may reveal the location of particles and relation between dispersed SiO$_2$ and SEBS-g-MA particles within the iPP matrix, and accordingly, the morphology of the iPP/SiO$_2$/SEBS-g-MA composites. The presented results confirm literature findings that the filler is not fully located only in one phase or only at the interface.[24]

Dark hollows in SEM micrographs are mainly related to the dispersed SEBS-g-MA particles at fractured surfaces. Bright spots originate from micron- and nano-sized silica particles and their aggregates. SEM micrographs in Figs. 2 and 3 indicate homogeneously dispersed SEBS-g-MA particles as well

TABLE 8

Overview of the morphologies predicted on the basis of proposed approaches

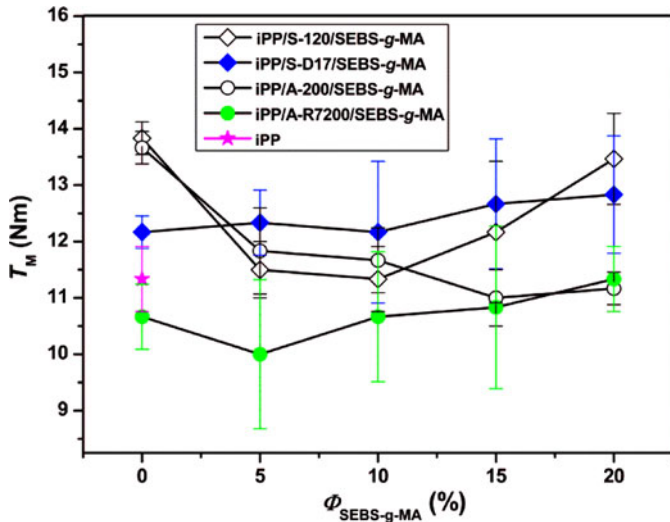| Approach	Possible morphologies of ternary composites iPP/silica/SEBS-g-MA			
	iPP/S-120/ SEBS-g-MA	iPP/SEBS-D17/ SEBS-g-MA	iPP/A-200/ SEBS-g-MA	iPP/A-R7200/ SEBS-g-MA
γ_{AB}, W_{AB}, S_{AB}	CS, cCs	iCS+SM	CS+cCS	CS+cCS+iCS
$\gamma_{AF} \geq \gamma_{BF}-\gamma_{AB}/2$; $\gamma_{BF} \geq \gamma_{AF}-\gamma_{AB}/2$	CS+cCS	iCS+SM	CS+cCS	iCS
ω_A	CS+cCS+iCS	iCS	CS+cCS+iCS	CS+cCS+iCS
λ_{AF}, λ_{AF}^*	CS+cCS	iCS+SM	CS+cCS	iCS+SM

FIG. 1. Torque moment T_M after 7 min of kneading for the iPP/SiO$_2$/SEBS-g-MA composites in dependence on the added amount of SEBS-g-MA elastomer.

as homogeneous distribution of silica microparticles and agglomerates in the iPP matrix phase. Large micron-sized S-120 and S-D17 silica particles ($d_{SiO2} > d_{SEBS-g-MA} \sim 3\,\mu m$) were mainly pulled out from fractured composite surfaces without encapsulation by SEBS-g-MA (large hollows probably originated from pulled out silica microparticles – Fig. 2b). Smaller micron-sized particles (up to $\sim 3\,\mu m$) remained within SEBS-g-MA holes at fractured surfaces forming a core-shell morphology (CS) (Figs. 2 and 3).

The agglomerates of tiny S-120 particles (smaller than 1 μm) filled the dark SEBS-g-MA holes, thus forming a preferentially complex compartmentalized core-shell or multiple inclusion morphology (cCS) in the iPP/S-120 composite with 10% of SEBS-g-MA (Figure 2a). The observed CS and cCS morphologies are in accordance with the morphologies

predicted by interfacial properties (Table 8). The iPP/S-120 composite with 20% of added SEBS-g-MA exhibits all kinds of core-shell morphologies: encapsulated micro-sized S-120 particles by SEBS-g-MA (CS) in Fig. 2b, compartmentalized core-shell morphology (cCS – upper inserted picture), and inverse core-shell morphology (iCS – bottom inserted picture).

The observed morphologies match well with the result obtained by the wetting coefficient approach (ω_a) (CS, cCS, iCS in Table 8). The spreading of the S-120 interlayers and the dispersion of silica agglomerates into a less viscous iPP phase was expected (MFR$_{iPP}$ = 6.0 g/min; MFR$_{SEBS-g-MA}$ = 3.1 g/10 min) in spite of the positive spreading coefficient of the SEBS-g-MA/S-120 higher than the one for the iPP/S-120 pair (Table 4).[22,28,31] Obviously, the real composite morphology changes somewhat with the increasing SEBS-g-MA content due to the increased influence of viscosity relative to the interfacial interactivity.

The iPP/S-D17 96/4 composite modified with the already 10% of SEBS-g-MA reveals small dark holes inside thick interlayers consisting of agglomerated submicron particles (Fig. 3a), unlike its composite analogue with polar S-120 microsilica (Fig. 2a). This may indicate a preferential inverse core-shell morphology (iCS) in composites with S-D17 as predicted by the results in Table 7. Thick interlayers of agglomerated particles suggest their spreading to the iPP matrix, thus confirming coexistence of iCS and SM morphologies predicted by the adhesion parameters (γ_{AB}, W_{AB}, S_{AB}), the interfacial free energy (γ_{AF}), and the Harkins spreading coefficients (λ_{AF}, λ_{AF}^*) (Table 8). Composites with S-D17 microsilica changes negligible with increasing elastomer content similarly to torque moment behavior of this system (Fig. 1).

Ternary composites with hydrophilic A-200 nanosilica (Fig. 4) exhibit morphologies similar to these with tiny hydrophilic S-120 silica particles (Fig. 2). Complex compartmentalized morphology (cCS) (the left micrograph in Fig. 4) prevails in the iPP/A-200 composite with 10 vol% of elastomer,
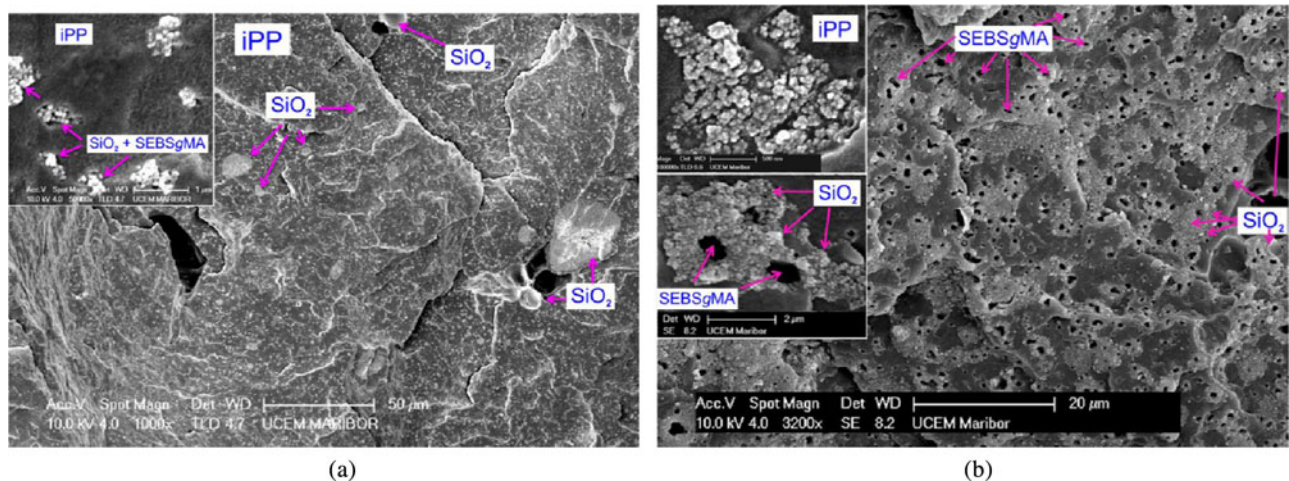

FIG. 2. SEM micrographs of the iPP/S-120 96/4 composites modified with 10% (a) and 20% (b) of added SEBS-g-MA.
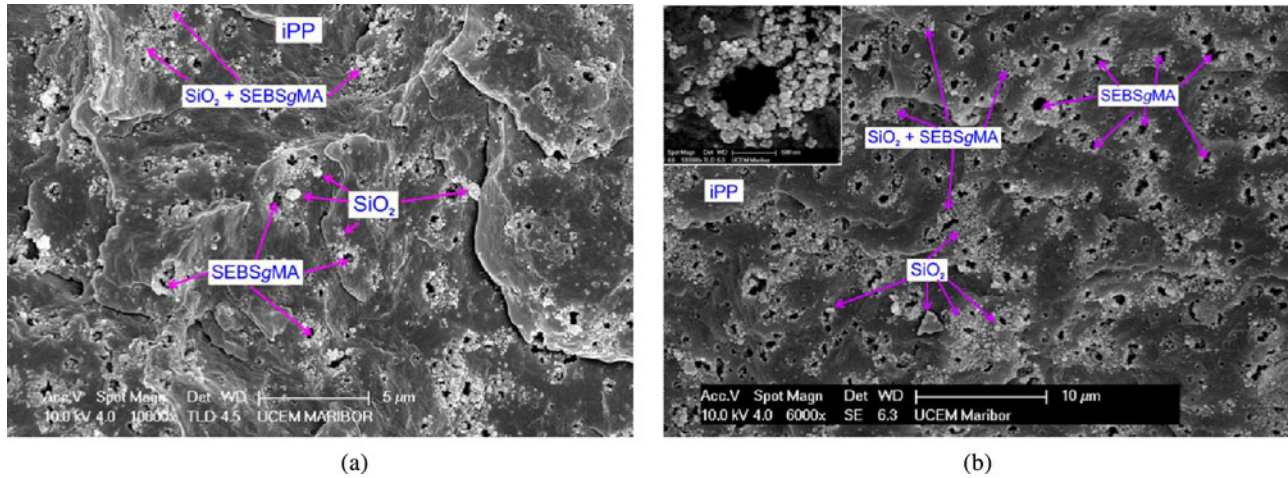
FIG. 3.   SEM micrographs of the iPP/S-D17 96/4 composites modified with 10% (a) and 20% (b) of added SEBS-g-MA reveal the preferential iCS morphology.
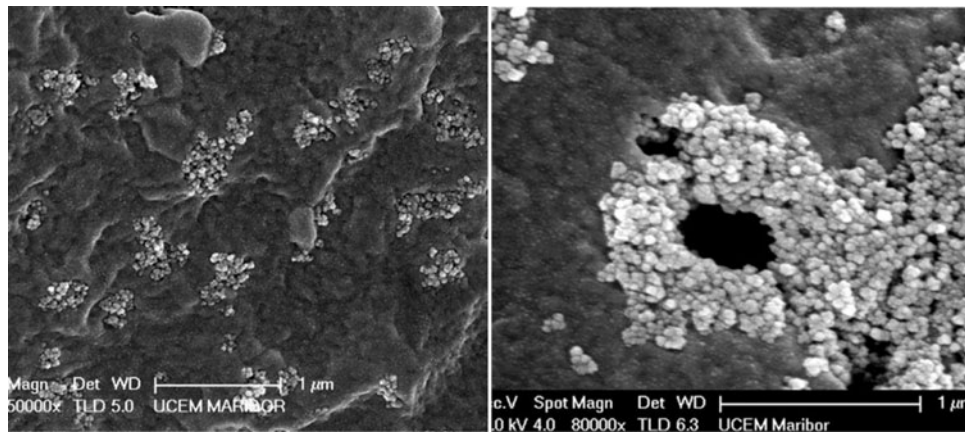

FIG. 4.   SEM micrograph of the iPP/A-200 96/4 composite with 10% (left) and 20% of added SEBS-g-MA (right).

whereas iCS and SM morphologies prevail in a composite with 20% of SEBS-g-MA (the right micrograph in Fig. 4). Real morphologies are in accordance with the predicted ones referred to in Table 7. The reason for the spreading of A-200 interlayers to the iPP matrix is the same as for S-120 submicron-sized particles. Morphological similarity of the composites to the A-200 and S-120 fillers obviously stem from the nucleating hydrophilic surfaces (–OH groups) of their particles.

Ternary composites with methacrylsilanized A-R7200 nanofiller exhibit all possible morphologies: Cs, cCS, iCS, SM (Fig. 5), thus confirming the morphologies predicted in Table 8. There are two specific features of these morphologies: huge nanosilica agglomerates and very irregular and complex morphologies. The interlayers of agglomerated A-R7200 nanoparticles indicate the most common appearance of iCS+SM morphologies like in the composite with S-D17 microsilica.

Generally, SEM micrographs of all presented composites reveal a spectrum of morphologies (CS, cCS, iCS, and SM)

with one or just two preferential morphologies in every sample (Figs. 2–5).

Spherulitic Morphology of iPP/SiO$_2$/SEBS-g-MA Composites

Polarized optical micrographs in Figs. 6a-c indicate two opposite, competitive effects on spherulite growth in the iPP matrix: the nucleation effect of the filler and the solidification effect of the SEBS-g-MA elastomer. The addition of all silica grades to plain iPP decreases the size of spherulite due to their nucleation ability.[15] Even the treated nonpolar S-D17 microsilica with minimal nucleation ability decreases the spherulite size, as illustrated by polarized optical micrographs in Figs. 6 a,b.

On the other hand, an increase in spherulite size with the increasing elastomer content (Fig. 6c) could be ascribed to the solidification effect. Namely, the crystallization of the iPP matrix during solidification of the molten iPP matrix was prolonged and enhanced due to the enabled migration of iPP chains from the remaining melt islands of the SEBS-g-MA elastomer.
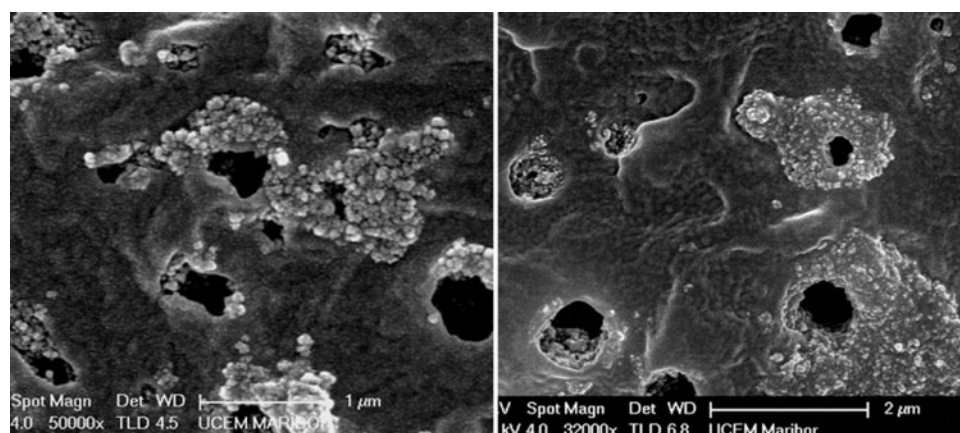
FIG. 5. SEM micrographs of the iPP/A-R7200 96/4 composites with 10% (left) and 20% (right) of added SEBS-*g*-MA reveal rather multiplex morphologies.
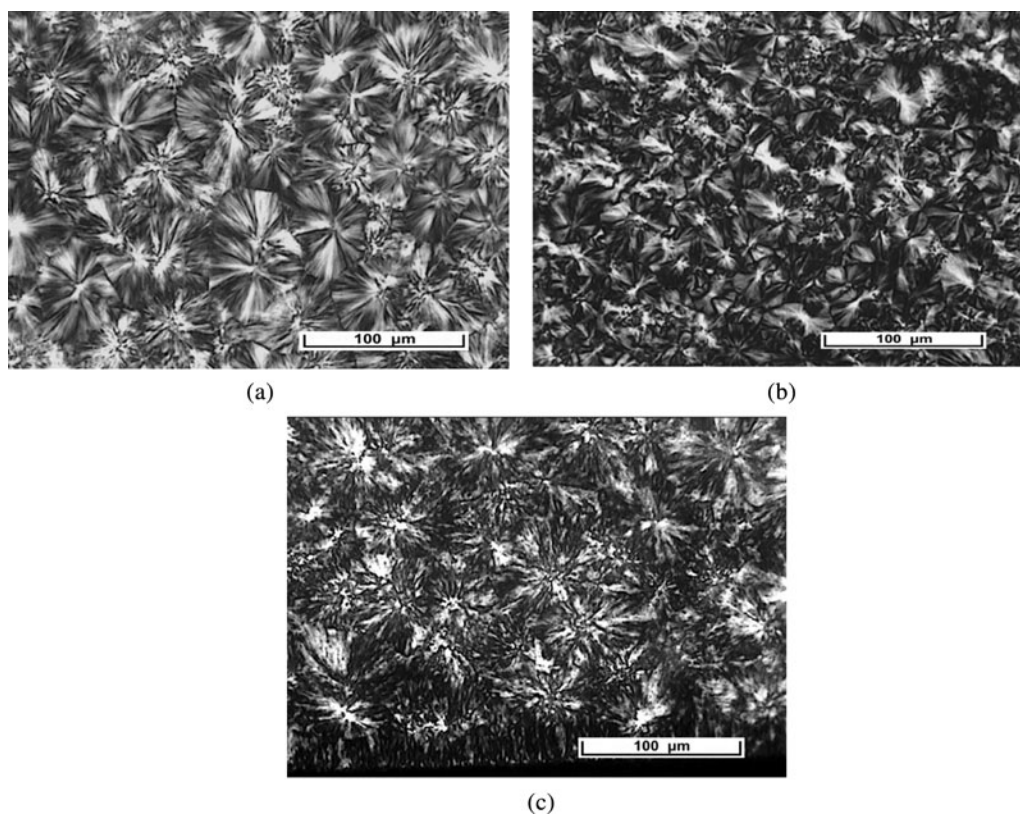

FIG. 6. Polarized optical micrographs of neat iPP (a), binary iPP/S-D17 96/4 composite (b), and ternary iPP/S-D17 96/4 + 20% SEBS-*g*-MA composite (c).

The spherulite size in the present composites with 20% of SEBS-*g*-MA ascends in the order: A-200 < S-120 < A-R7200 < S-D17. The largest spherulites were observed in composites containing the S-D17 non-polar silica filler that exhibits the weakest nucleation ability because its surface is compatible with the iPP matrix.[15,32] Preferential iCS and SM morphologies with a significant iPP−S-D17 interface area may reduce nucleation and additionally enhance the spherulite growth.

The optical micrographs of the iPP/S-D17 96/4 composite modified with 10% and 20% of added SEBS-*g*-MA elastomer (the left and right micrographs in Fig. 7) illustratively exhibit the accommodation of dispersed elastomer and filler particles in relation to the iPP spherulites. These micrographs also confirm homogeneously dispersed SEBS-*g*-MA particles as well as homogeneous distribution of silica microparticles in the iPP matrix phase. Dispersed elastomeric SEBS-*g*-MA particles
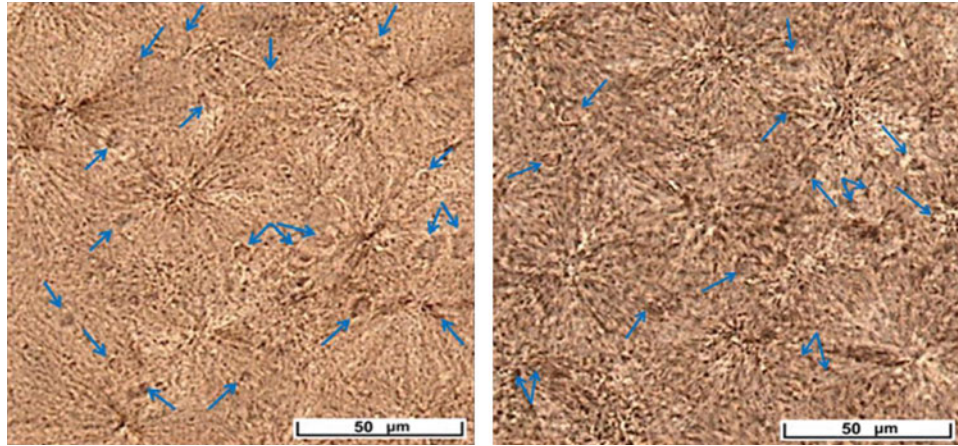
FIG. 7. Optical micrographs of iPP/S-D17 96/4 microcomposite modified with 10% (left) and 20% (right) of SEBS-g-MA. The arrows show the largest micron-sized S-D17 particles discernible under the ocular as a result of additional magnification.

are accommodated more intraspherulitically than interspherulitically even in composites with 20% of SEBS-g-MA (dark spots of average size $d_p \sim 2$–3 µm).

This accommodation possibility was also observed by Karger–Kocsis et al.[33] in the PP/EPDM blends. Radial intraspherulitical alignment of dispersed SEBS-g-MA particles may indicate the preferentially radial accommodation of dispersed SEBS-g-MA particles between growing lamellae or between bundles of lamellae during their crystallization (dark spots in Figs. 6 and 7). A somewhat higher concentration of these spots in bigger spherulites (not shown) may confirm the influence of molten elastomeric islands on the spherulite growth during solidification. The S-D17 silica microparticles, larger than the dispersed SEBS-g-MA particles up to one order of magnitude, are mostly separated in the iPP matrix. Some optical micrographs reveal sporadic dark spots of elastomer particles at the iPP−S-D17 interface. The prevailing interspherulitic alignment of micro-sized S-D17 particles in this ternary composite cannot explain whether these microparticles are ejected to the spherulite surfaces or they stop the spherulite growth regardless of their nucleation ability.

Tensile Properties

Mechanical properties of reinforced polymer-matrix composites are primarily influenced by component properties and interfacial interaction between the polymer matrix and the dispersed filler and elastomer particles, as well as by the ultimate morphology of composites.[1,2]

Young's Modulus

The effect of the SEBS-g-MA content on Young's modulus (E), as a measure of composite stiffness, is shown in Fig. 8. The E value of all ternary iPP/SiO₂/SEBS-g-MA composites steadily decreases upon addition of the SEBS-g-MA elastomer. An almost linear decrease in the E values is in accordance with the parallel model[31]. The similarity in the E-Φ behavior

of samples to different fillers indicates two competitive effects: stiffening effect of the filler and toughening effect of the elastomer[34] rather than morphological or microstructural effects on Young's modulus[6]. Because the addition of silica filler to the iPP usually increases the stiffness of binary composites[16], the decrease in the E values in ternary composites is obviously caused by a prevailing toughening effect of the SEBS-g-MA elastomer. The convergence of the E values with the increasing elastomer content confirms the enhancing impact of the elastomer.

Tensile Strength and Elongation at Break

As the incorporation of different fillers into polymers affects tensile strength at break, σ_b. Unlike that, the addition of both fillers and modifiers to the matrix has a more complex impact;[1,2] they may either increase or decrease σ_b values or
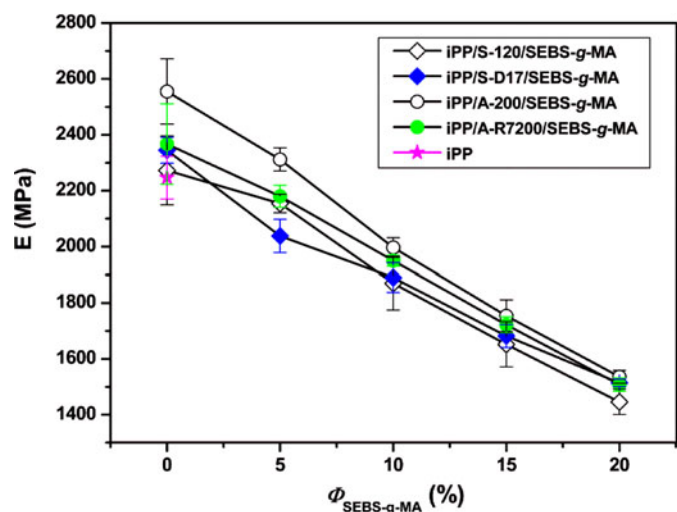

FIG. 8. Young's modulus E of ternary iPP/SiO₂/SEBS-g-MA composites in dependence on added amount of SEBS-g-MA elastomer.
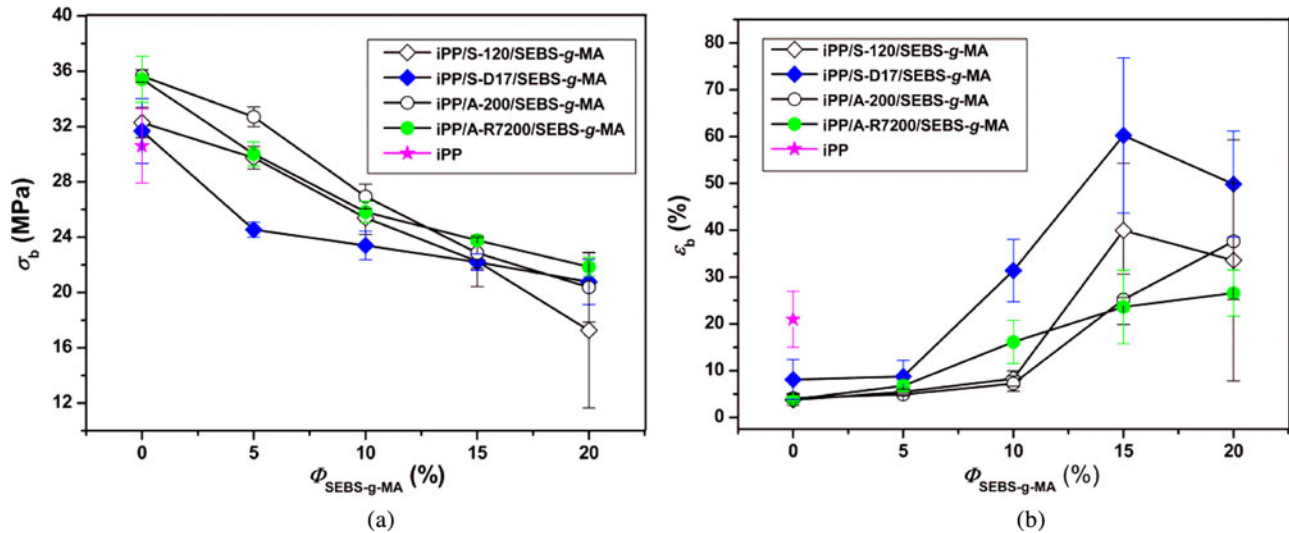
FIG. 9.   Tensile strength σ_b (a) and elongation at break ε_b(b) of the iPP/SiO$_2$/SEBS-g-MA composites in dependence on the added amount of SEBS-g-MA elastomer.

behave without any visible effect on tensile strength[5]. The σ_b values of ternary iPP/SiO$_2$/SEBS-g-MA composites decrease with the steadily increasing elastomer content (Fig. 9a). The composites with modified fillers (S-D17, A-R7200) exhibit somewhat lower σ_b values than those with untreated parent fillers (S-120, A-200) up to 15% of added SEBS-g-MA modifier.

The elongation at break, ε_b, usually behaves inversely to the tensile strength at break. The ε_b values increase with the increasing SEBS-g-MA content but not exactly in the inverse mode (Fig. 9b). It is interesting that the ε_b values of composites containing microsized fillers behave similarly – they increase up to 15% of added SEBS-g-MA and then decline. Higher ε_b values for microcomposites than for nanocomposites

FIG. 10.   Notched impact strength a_k of the iPP/SiO$_2$/SEBS-g-MA composites in dependence on the added amount of SEBS-g-MA.

(Fig. 9b) correspond to a similar steady torque moment behavior at the higher SEBS-g-MA content (Fig. 1). Moreover, the highest ε_b values for the composite with nonpolar S-D17 microsilica (Fig. 9b) may be merely attributed to enlarged spherulites in this composite (Fig. 6c).

Impact Properties

The incorporation of the silica filler improves some mechanical properties of the iPP (such as stiffness, tensile strength), but it usually reduces toughness, which leads to a poorer impact strength[16]. The SEBS-g-MA elastomer was added to the binary iPP/SiO$_2$ composites as impact modifier in order to increase its toughness. Therefore, the proper balance of the mechanical behavior of such polymer-matrix composite materials may be achieved by a proper combination of selected components.

Although the addition of fillers to the iPP decreases the notched impact strength, the addition of the SEBS-g-MA elastomer to the iPP/SiO$_2$ composites steadily increases a_K values (Fig. 10). Thus the composites containing 20% of loaded elastomer exhibit a four- to five-fold increase in the a_K values compared with binary composites and approximately three-fold increase in a_K values compared with neat polypropylene. This fact indicates a significant overcoming of the elastomeric toughening effect in relation to the filler's stiffening effect. The a_K values of all four composite systems are very close; the similarity of a_K-Φ to the E-Φ feature of all samples indicates a combined effect (stiffening by filler and toughening by elastomer) rather than a morphological effect on these mechanical properties.

CONCLUSIONS

The results (predicted and observed morphologies) of presented iPP/SiO$_2$/SEBS-g-MA composites confirm literature
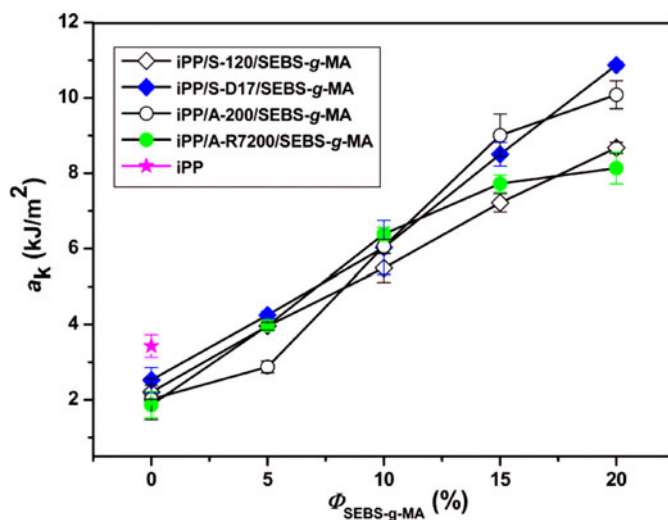
TABLE 9
Comparison of the morphologies of iPP/SiO$_2$/SEBS-*g*-MA composites with different fillers

	Overview of iPP/silica/SEBS-*g*-MA morphologies		
Ternary polymer composites	Morphologies predicted with calculation of adhesion parameters	Observed morphologies	Preferential morphologies
iPP/S-120/SEBS-*g*-MA	CS+cCS+iCS	CS+cCS+iCS	cCS
iPP/A-200/SEBS-*g*-MA	CS+cCS+iCS	CS+cCS+iCS	cCS
iPP/S-D17/SEBS-*g*-MA	iCS+SM	SM+iCS	iCS, SM
iPP/S-D17/SEBS-*g*-MA	CS+cCS+iCS	CS+cCS+iCS	iCS, SM

findings that the morphology of every composite is a spectrum of several morphologies rather than one exclusive morphology.[24] The composites with untreated surfaces silica fillers (S-120, A-200) exhibit similar cCS morphology (Table 9) as preferential due to stronger interfacial interaction between SEBS-*g*-MA– silica than iPP – silica surfaces. The composites with treated surfaces of silica fillers (S-D17, A-R7200) exhibited similar coexistence of iCS and SM morphology as preferential (Table 9) due to somewhat stronger interfacial interaction between iPP – silica than SEBS-*g*-MA– silica surfaces.

Generally, an outstanding influence of competitive nucleation and solidification effects of the filler and the elastomer on spherulite growth has been observed. Ascending of the spherulite size in the present composites in the order: A-200 < S-120 < A-R7200 < S-D17 may indicate an additional influence of preferential iCS and SM morphologies in composites with S-D17 and A-R7200 on reduced nucleation and enhanced growth of spherulites. Dispersed SEBS-*g*-MA particles are accommodated intraspherulitically and interspherulitically. The intraspherulitically aligned SEBS-*g*-MA particles seem to follow the radial accommodation of molten SEBS-*g*-MA islands in the radial direction of growing lamellae during crystallization. The tensile and impact strength properties were influenced by competitively opposite effects of the stiff filler and the toughened SEBS-*g*-MA elastomer rather than by other factors.

REFERENCES

1. Rothon, R.N. *Particulate-Filled Polymer Composites*, 2nd ed., Rapra Techology: Shawbury, United Kingdom, 2006.
2. Wypych, G. *Handbook of Fillers*, 2nd ed., ChemTec Publishing: Toronto, 2000.
3. Wagner, M.P. *Additives for Plastics*, Academic Press: New York, 1978; pp. 9–28.
4. Bikiaris, D.N.; Vassiliou, A.; Pavlidou, E.; Karayannidis, G.P. Compatibilisation effect of PP-g-MA copolymer on iPP/SiO$_2$ nanocomposites prepared by melt mixing. Eur. Polym. J. **2005**, *41*, 1965–1978.
5. Chen, J.H.; Rong, M.Z.; Ruan, W.H.; Zhang, M.Q. Interfacial enhancement of nano-SiO$_2$/polypropylene. Compos. Sci. Technol. **2009**, *69*, 252–259.
6. Uotila, R.; Hippi, U.; Paavola, S.; Seppala, J. Compatibilization of PP/elastomer/microsilica composites with functionalized polyolefins: effect on microstructure and mechanical properties. Polymer **2005**, *46*, 7923–7930.
7. Martin, G.; Barres, C.; Sonntag, P.; Garois, N.; Cassagnau, P. Co-continuous morphology and stress relaxation behaviour of unfilled and silica filled PP/EPDM blends. Mater. Chem. Phys. **2009**, *113*, 889–898.
8. Bazgir, S.; Katbab, A.A.; Nazockdast, H. Silica-reinforced dynamically vulcanized ethylene–propylene–diene monomer/polypropylene thermoplastic elastomers: Morphology, rheology, and dynamic mechanical properties. J. Appl. Polym. Sci. **2004**, *92*, 2000–2007.
9. Liu, Y.; Kontopoulou, M. The structure and physical properties of polypropylene and thermoplasticolefin nanocomposites containing nanosilica. Polymer **2006**, *47*, 7731–7739.
10. Wang, W.-Z.; Liu, T. Mechanical properties and morphologies of polypropylene composites synergistically filled by styrene-butadiene rubber and silica nanoparticles. J. Appl. Polym. Sci. **2008**, *109*, 1654–1660.
11. Mae, H.; Omiya, M.; Kishimoto, K. Comparison of mechanical properties of PP/SEBS blends at intermediate and high strain rates with SiO$_2$ nanoparticles Vs. CaCO$_3$ fillers. J. Appl. Polym. Sci. **2008**, *110*, 1145–1157.
12. Panaitescu, D.M.; Vulunga, Z.; Notingher, P.V.; Nicolae, C. The effect of poly[styrene-b-(ethylene-co-butylene)-b-styrene] on dielectric, thermal, and morphological characteristics of polypropylene/silica nanocomposites. Polym. Eng. Sci. **2013**, *53*, 2081–2092.
13. Panaitescu, D.M.; Vulunga, Z.; Radovici, C.; Nicolae, C. Morphological investigation of PP/nanosilica composites containing SEBS. Polym. Test. **2012**, *31*, 355–365.
14. EL-Midany, A.A.; Ibrahim, S.S. Interfacial role of compatibilizers to improve mechanical properties of silica– Polypropylene composites. Probl. Miner. Process. **2010**, *46*, 295–305.
15. Pustak, A.; Pucić, I.; Denac, M.; Švab, I.; Pohleven, J.; Musil, V.; Šmit, I. Morphology of polypropylene/silica nano- and microcomposites. J. Appl. Polym. Sci. **2013**, *128*, 3099–3106.

16. Pustak, A.; Denac, M.; Leskovac, M.; Švab, I.; Makarovič, M.; Musil, V.; Šmit, I.J. Reinf. Plast. Compos. **2014**, *33*, 851–861.

17. Ström, G.; Fredriksson, M.; Stenius, P. Contact angles, work of adhesion, and interfacial tensions at a dissolving hydrocarbon surface. J. Coll. Interf. Sci. **1987**, *119*, 352–361.

18. van Oss, C.J.; Giese, RF.; Li, Z.; Murphy, K.; Norris, J.; Chaudhury, M.K.; Good, R.J. *Contact Angle, Wettability and Adhesion*, VSP: Utrecht, 1993; pp. 269–284.

19. Wu, S. Polar and nonpolar interaction and nonpolar interaction in adhesion. J. Adhes. **1973**, *5*, 39–55.

20. Mittal, K.L. The role of the interface in adhesion phenomena. Polym. Eng. Sci. **1977**, *17*, 467–473.

21. Urashita, S.; Kawakatsu, T.; Doi, M. Prediction of the domain structure in ternary polymer blend. Prog. Theor. Phys. Suppl. **2000**, *138*, 412–417.

22. Premphet, K.; Horanont, P. Phase structure of ternary polypropylene/elastomer/filler composites: effect of elastomer polarity. Polymer **2000**, *41*, 9283–9290.

23. Work, W.J.; Horie, K.; Hess, M.; Stepto, R.F.T. Definition of terms related to polymer blends, composites, and multiphase polymeric materials. IUPAC Pure Appl. Chem. **2004**, *76*, 1985–2007.

24. Steinmann, S.; Gronski, W.; Friedrich, C. Influence of selective filling on rheological properties and phase inversion of two-phase polymer blends. Polymer **2002**, *43*, 4464–4467.

25. Ma, C.G.; Mai, Y.; Rong, M.Z.; Ruan, W.H.; Zhang, M.Q. Phase structure and mechanical properties of ternary polypropylene/elastomer/nano-CaCO$_3$ composites. Compos. Sci. Technol. **2007**, *67*, 2997–3005.

26. Reignier, J.; Favis, B.D.; Heuzey, M.-C. Factors influencing encapsulation behavior in composite droplet-type polymer blends. Polymer **2003**, *44*, 49–59.

27. Clarke, J.; Clarke, B.; Freakley, P.K.; Sutherland, I. Compatibilising effect of carbon black on morphology of NR-NBR. Plast. Rubber. Compos. **2001**, *30*, 39–44.

28. Sumita, M.; Sakata, K.; Asai, S.; Miyasaka, K.; Nakagawa, K.H. Dispersion of fillers and the electrical conductivity of polymer blends filled with carbon black. Polym. Bull. **1991**, *25*, 265–271.

29. Hobbs, S.Y.; Dekkers, M.E.J.; Watkins, V.H. Effect of interfacial forces on polymer blend morphologies. Polymer **1988**, *29*, 1598–1602.

30. Das, S.; Murthy, V.S.R.; Murty, G.S. Particulate size effect on the rheology of SiC-glass composites. J. Mater. Sci. **1999**, *34*, 1347–1352.

31. Gedde, U.W. *Polymer Physics*, Chapman and Hall: London, 1996; Chapter 9.

32. Ray, S.S.; Bandyopadhyay, J.; Bousmina, M. Influence of degree of intercalation on the crystal growth kinetics of poly[(butylene succinate)-co-adipate] nanocomposites. Eur. Polym. J. **2008**, *44*, 3133–3145.

33. Karger-Kocsis, J.; Kiss, L.; Kuleznev, V.N. Optical microscopic study on the phase separation of impact modified polypropylene blends and polypropylene block copolymer. Polym. Commun. **1984**, *25*, 122–126.

34. Hornsby, P.R.; Premphet, K. Influence of phase microstructure on the mechanical properties of ternary phase polypropylene composites. J. Appl. Polym. Sci. **1998**, *70*, 587–597.